Full radius linear and nonlinear gyrokinetic simulations for tokamaks and stellarators: zonal flows, applied $\boldsymbol{E} \times \boldsymbol{B}$ flows, trapped electrons and finite beta

2004 Nucl. Fusion 44 172

(http://iopscience.iop.org/0029-5515/44/1/019)

INSTITUTE OF PHYSICS PUBLISHING and INTERNATIONAL ATOMIC ENERGY AGENCY NUCLEAR FUSION

Nucl. Fusion **44** (2004) 172–180 PII: S0029-5515(04)72614-9

Full radius linear and nonlinear gyrokinetic simulations for tokamaks and stellarators: zonal flows, applied $E \times B$ flows, trapped electrons and finite beta

L. Villard[1], S.J. Allfrey[1], A. Bottino[1], M. Brunetti[1], G.L. Falchetto[2], V. Grandgirard[2], R. Hatzky[3], J. Nührenberg[4], A.G. Peeters[5], O. Sauter[1], S. Sorge[4] and J. Vaclavik[1]

[1] Centre de Recherches en Physique des Plasmas, Ecole Polytechnique Fédérale de Lausanne, Euratom-Suisse, Lausanne, Switzerland
[2] Département de Recherches sur la Fusion Côntrôlée, Euratom-CEA, Cadarache, France
[3] Rechenzentrum der Max-Planck Gesellschaft, Garching, Germany
[4] Max-Planck Institut für Plasmaphysik, Euratom-IPP, Greifswald, Germany
[5] Max-Planck Institut für Plasmaphysik, Euratom-IPP, Garching, Germany

E-mail: laurent.villard@epfl.ch

Received 16 October 2002, accepted for publication 11 November 2003
Published 17 December 2003
Online at stacks.iop.org/NF/44/172 (DOI: 10.1088/0029-5515/44/1/019)

Abstract
The aim of this paper is to report on recent advances made in global gyrokinetic simulations of ion temperature gradient (ITG) modes and other microinstabilities. The nonlinear development and saturation of ITG modes and the role of $E \times B$ zonal flows are studied with a global nonlinear δf formulation that retains parallel nonlinearity and thus allows for a check of the energy conservation property as a means of verifying the quality of the numerical simulation. Due to an optimized loading technique, the conservation property is satisfied with an unprecedented quality well into the nonlinear stage. The zonal component of the perturbation evolves to a quasi-steady state with regions of ITG suppression, strongly reduced radial energy flux and steepened effective temperature profiles alternating with regions of higher ITG mode amplitudes, larger radial energy flux and flattened effective temperature profiles. A semi-Lagrangian approach free of statistical noise is proposed as an alternative to the nonlinear δf formulation. An ASDEX-Upgrade experiment with an internal transport barrier is analysed with a global gyrokinetic code that includes trapped electron dynamics. The weakly destabilizing effect of trapped electron dynamics on ITG modes in an axisymmetric bumpy configuration modelling W7-X is shown in global linear simulations that retain the full electron dynamics. Finite β effects on microinstabilities are investigated with a linear global spectral electromagnetic gyrokinetic formulation. The radial global structure of electromagnetic modes shows a resonant behaviour with rational q values.

PACS numbers: 52.30.Gz, 52.35.Qz, 52.35.Mw, 52.35.Ra

1. Introduction

Ion temperature gradient (ITG) modes and other microinstabilities are the physics basis of several gyrofluid or gyrokinetic models that attempt to describe anomalous transport in magnetically confined plasmas [1]. The prominent role of zonal flows in ITG saturation was recognized already some time ago in gyrofluid [2] and gyrokinetic [3, 4] simulations. Through nonlinear coupling of ITG modes, a component of the electric field normal to the magnetic surfaces is driven. The $E \times B$ drift of this component, in other words the zonal $E \times B$ flow, in turn reduces the level of ITG turbulence. Thus the zonal component of the perturbation appears as a regulator of the ITG turbulence. The zonal flow has a linearly undamped component [5], and its interaction with turbulence is purely nonlinear in collisionless models. Since the turbulence level is ultimately determined by this nonlinear interaction, it should be ensured that the numerical discretization scheme does not introduce unphysical mechanisms affecting this dynamics. At this point the check of energy and particle conservation properties [6]

becomes an extremely useful and stringent test of the quality of the numerical simulation.

Methods based on the PIC δf method [7] have been used widely to solve the gyrokinetic equations. Satisfying energy conservation has proved to be technically rather difficult. The main obstacle is to reduce the numerical noise inherent to such methods down to an acceptable level; in other words, the challenge is to have a good enough statistic for the gyrocentre tracers. While the parallel nonlinearity was neglected in some works, thus relinquishing the underlying energy conservation properties, it was only recently that energy conservation was demonstrated in nonlinear full-radius gyrokinetic simulations, the result of an optimized loading technique that uses the energy conservation as an indicator of the numerical quality [8–11]. Results of the application of this method are presented in section 2 and compared with results without optimization. The consequences of neglecting the parallel nonlinearity are also shown. A 'semi-Lagrangian' formulation is introduced as an alternative to the PIC δf approach.

More physical effects appear when not only the ion, but also the electron dynamics, are taken into account. In section 3, we show the application of a model that assumes adiabatic passing electrons and drift-kinetic trapped electrons to the study of $E \times B$ stabilization in an ASDEX-Upgrade shot with an internal transport barrier (ITB). Then a model that includes the full electron dynamics is applied to a bumpy cylindrical configuration relevant for W7-X parameters. When finite plasma β is taken into account, the microinstabilities become electromagnetic in character. As the toroidal-ITG mode is stabilized with increasing β, another mode called the kinetic ballooning mode [12] or Alfvénic ITG (AITG) [13] is destabilized with a threshold value below the ideal MHD ballooning limit. We show the results of a global spectral gyrokinetic approach that has allowed us to find a remarkable resonant behaviour of the AITG mode radial structure with rational q values. Finally, the main findings and possible future work are discussed in section 4.

2. Energy conserving simulations of ITG modes and zonal $E \times B$ flows

In this section, we consider a straight cylindrical configuration. The parameters are pertinent to W7-X: $B_0 = 2.5\,\mathrm{T}$, $a = 0.55\,\mathrm{m}$, $T_\mathrm{i} = 5\,\mathrm{keV}$, deuterium (thus $a = 135\rho_\mathrm{Li}$), uniform density and T_e profiles, ITG with $a/L_\mathrm{T} = 3$ peaking at mid-radius. We solve the gyrokinetic equations for ions and a quasi-neutrality equation assuming an adiabatic electron response within cylindrical surfaces. In addition to the $E \times B$ nonlinearity, the $v_\parallel$ nonlinearity is retained and thus an energy conservation principle is satisfied:

$$\begin{aligned} \mathcal{E}_\mathrm{kin} &= \int \frac{1}{2} m_\mathrm{i} v^2 f \,\mathrm{d}\boldsymbol{R}\,\mathrm{d}\boldsymbol{v}, \\ \mathcal{E}_\mathrm{field} &= \int \frac{q_\mathrm{i}}{2} \left(\langle n_\mathrm{i}\rangle - n_0\right) \phi \,\mathrm{d}\boldsymbol{x}, \\ \frac{\mathrm{d}}{\mathrm{d}t}(\mathcal{E}_\mathrm{kin} + \mathcal{E}_\mathrm{field}) &= 0, \end{aligned} \tag{1}$$

where $\langle\ \rangle$ indicate a gyro-averaged quantity. A finite element, PIC δf method is used [14]. Pseudo-randomly chosen points in phase space, or 'tracers', are evolved according to the gyrocentre trajectories. The quasi-neutrality equation is solved using a finite element method. The right-hand side of the quasi-neutrality equation is calculated by projecting the gyro-averaged ion density represented by the tracers onto a finite element basis. Statistical noise is inherent to the method. The use of a δf approach [7], in which only the perturbed part of the distribution function is used in calculating the right-hand side of the quasi-neutrality equation, greatly reduces numerical noise. By writing $f = f_0 + \delta f$, with f_0 a known background function, the statistical approximation is made not for f but only δf, a function of much lower variance. However, the method can be further improved. The optimized loading technique [8] consists of choosing a distribution of the gyrocentres that minimizes this statistical noise. First, a numerical simulation is run with a tracer density proportional to an equilibrium Maxwellian up to a point before the quality of the simulation becomes poor, with the energy conservation serving as an indicator of the quality. The values of $|\delta f|$ are back-mapped to the original tracer positions at time $t = 0$, and a new distribution of tracers is generated from this data. Then a new simulation is performed starting with the new tracer distribution. Eventually, the whole process can be repeated until the desired accuracy is obtained. The bottom line is to increase the density of tracers in active regions of phase space.

We show in figure 1 the effect of loading optimization on the energy conservation, average radial heat flux and zonal component of the electric field, E_{r00}. Both simulations have been run using $2^{27} \approx 134$ million gyrocentre tracers and the same radial mesh, $N_\mathrm{r} = 64$, poloidal Fourier modes $m \in [-96, +96]$ and parallel Fourier modes $n_\parallel \in [-6, +6]$. These numerical parameters were chosen so as to ensure that all physically relevant modes are represented numerically. It is obvious that the optimization leads to an excellent energy conservation. A detailed analysis of the reasons for the optimized loading scheme to reduce the statistical error in such a drastic manner has been made. In the case of the simulation shown here, phase space activity (i.e. regions of phase space where $|\delta f|$ is large) takes place mostly between two and three ion thermal velocities and is also localized at certain radial positions. The gain in accuracy of the optimized loading thus comes from a better sampling in both velocity and configuration space.

A striking feature is that important physical quantities obtained with the proportional loading start to deviate from the physically more correct results as soon as the energy is not conserved ($t > 150\,\mu\mathrm{s}$). In the non-optimized, non-energy conserving simulation, the heat flux is a factor of more than 2 too high in the nonlinear stage at the end of the simulation (figure 1, middle). This large effect on the predicted heat flux level can be attributed to incorrect calculation of the zonal component of the electric field: we observe that the regular pattern of E_{r00} as computed with the energy conserving simulation (figure 1, bottom right) is destroyed at later times in the non-optimized, non-energy conserving simulation (figure 1, top right). Snapshots around $t = 300\,\mu\mathrm{s}$ of the ITG and zonal component of the electric field (figure 2) show a remarkable structure, with regions of positive E_{r00} coinciding with suppressed ITG mode activity and regions of negative E_{r00} in which ITG modes have a larger amplitude. The effective ion temperature profile is steepened in the suppressed ITG regions and flattened in the active ITG

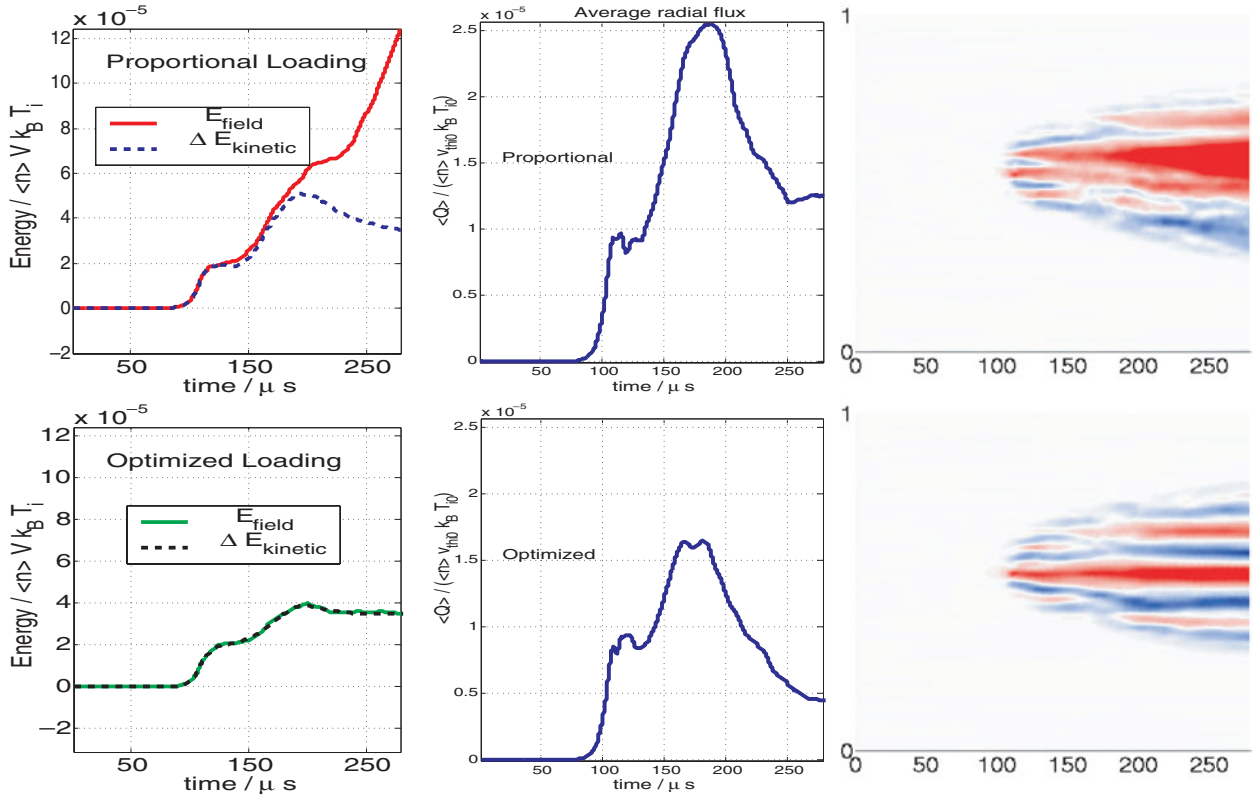

Figure 1. Field and kinetic energy (left), average radial heat flux (middle) and zonal $E \times B$ component $E_{r00}(r, t)$ (right, red for positive, max $= 24 \times 10^3\,\mathrm{V\,m^{-1}}$, blue for negative, min $= -24 \times 10^3\,\mathrm{V\,m^{-1}}$) versus time, for an unoptimized (proportional) loading (top) and after loading optimization (bottom).

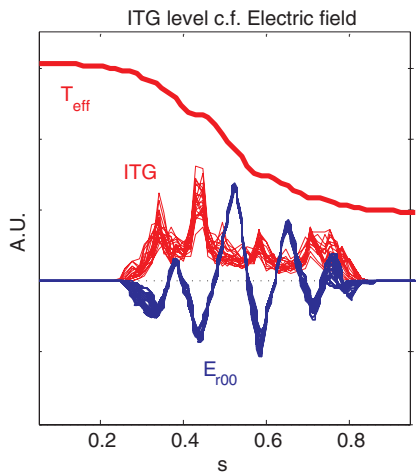

Figure 2. Snapshots of zonal $E \times B$ flow, ITG amplitude and effective temperature profiles well into the nonlinear stage of the optimized simulation of figure 1 around $t = 300\,\mu$s.

regions. The results of figure 2 may be surprising in that there appears an asymmetry with respect to the sign of E_{r00}, whereas linear calculations do not exhibit such an asymmetry. Also, it could be expected that turbulence is suppressed in all regions where the shearing rate is large: this is not the case here. We have actually verified, in linear computations in the presence of a fixed (equilibrium) radial electric field of a shape similar to that found in figure 2, that the most unstable ITG modes tend to localize in regions of vanishing shearing rate and that there is symmetry about the sign of E_{r00}. But the results of figures 1–3 are nonlinear. In particular, the zonal structure of the radial electric field is generated by the turbulence and not imposed as an equilibrium quantity. Also, the effective temperature profile is not frozen but is left free to evolve, and it does (see figure 2). There is no way to understand the results of figure 2 with arguments based solely on linear physics.

We note that at the end of the optimized simulation of figure 1, the system has not yet reached a steady-state everywhere in the plasma: there is still an evolution of the ITG and zonal perturbations at the inner and outer edges ($s <\approx 0.25$ and $s >\approx 0.75$). Continuing the optimized simulation further [15] until $t = 400\,\mu$s, which corresponds roughly to 40 turbulence decorrelation times, we find that the zonal perturbation structure remains steady, the average heat flux is constant to within $\pm 10\%$ and the energy conservation is satisfied to within less than 20% of the perturbed field energy. Thus the optimized loading technique is a means of getting numerical results that remain physically correct for longer times, deeper and deeper into the nonlinear regime, due to the noise reduction. In [15], a detailed analysis of statistical errors of the PIC method is presented and a revisited δf scheme is shown as a possible way to further improve the accuracy of the simulations.

We have confirmed the pivotal role of the zonal component of the electric field in artificially suppressing it: we have found a radial heat flux an order of magnitude higher. This seems to imply that the strongest nonlinearity in the system is the $E \times B$ nonlinearity. However, one should not conclude that

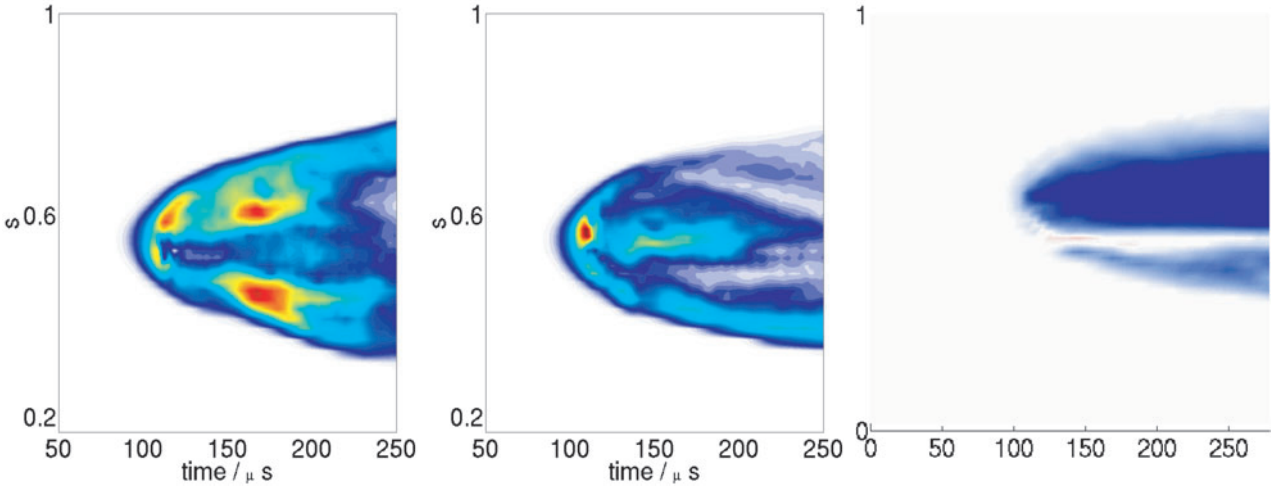

Figure 3. Radial heat flux versus time and radius with (left) and without (middle) $v_\parallel$ nonlinearity. Colour scale from blue (minimum value = 0) to red (maximum value = $4 \times 10^{-5} \bar{n} v_{\mathrm{thi}} k_{\mathrm{B}} T_{\mathrm{i}}$, where $\bar{n}$ is the volume averaged density). Zonal component of the electric field, E_{r00}, versus time and radius without $v_\parallel$ nonlinearity (right, red for positive, max = 48×10^3 V m^{-1}, blue for negative, min = -48×10^3 V m^{-1}).

the $v_\parallel$ nonlinearity is negligible. The main consequences of ignoring it are the absence of parallel ion trapping, therefore affecting nonlinear ion Landau damping, but more importantly, the charge conservation property not being satisfied. If there is no charge conservation, it has a large effect on the quasi-neutrality equation for the zonal component, which is a Poisson type of equation (unlike the $m \neq 0, n \neq 0$ components, for which the quasi-neutrality equation is a Helmoltz type). Thus the zonal $E \times B$ flows is incorrectly calculated, and this affects the predicted heat flux as well. Another consequence of neglecting the $v_\parallel$ nonlinearity is that the energy conservation property is not satisfied, and therefore a precious indicator of the quality of the numerics is lost. We performed a simulation with the same physical and numerical parameters as the optimized loading simulation of figure 1 but cancelling the term $(q_{\mathrm{i}}/m_{\mathrm{i}})\langle \boldsymbol{E} \rangle \cdot \boldsymbol{e}_\parallel$ in the equation for $\mathrm{d}v_\parallel/\mathrm{d}t$. The results were strongly affected by this modification. A Fourier decomposition of the field energy shows in particular that all components with $m = 0, n \neq 0$ are entirely unpopulated. The zonal $E_{r00}(r, t)$ pattern is strongly affected and with it the radial heat flux (figure 3). (Note that a similar important role of the parallel velocity nonlinearity, but on electrons, was found in the case of drift wave turbulence [16].)

An alternative to the PIC δf method is the semi-Lagrangian approach. This method retains both an Eulerian aspect in that the phase space is discretized on a fixed grid and a Lagrangian aspect in that the gyrocentre trajectories are computed (characteristics) to obtain the evolution of the full distribution function, f. The integration along characteristics is performed with a time-splitting algorithm that allows one to divide the resolution of the advection equation as a succession of two- and one-dimensional advections. Cubic spline interpolations are performed to evaluate the value of f at the feet of the characteristics. Preliminary results [17, 18] of a new code written for the cylindrical geometry and assuming drift-kinetic ions and adiabatic electrons show that the linear properties are well reproduced, that the zonal flows indeed have a prominent role in the saturation mechanism (see figure 4)

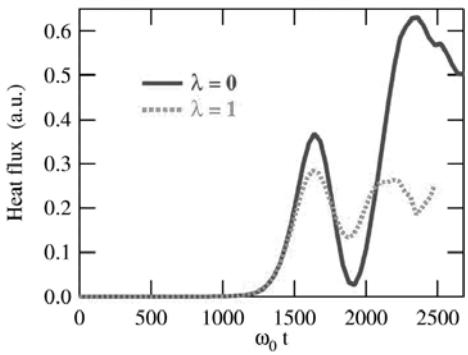

Figure 4. Heat flux without (——) and with (- - - -) zonal flows, obtained in a semi-Lagrangian nonlinear drift-kinetic simulation.

and that the energy conservation property can be satisfied with reasonable accuracy. The parameters used in these computations were for a small cylinder plasma of radius $10\rho_{\mathrm{Li}}$, constant density and T_{e} profiles, a T_{i} profile with maximum gradient at mid-radius and $a/L_{\mathrm{T}} = 4$. The reasons for choosing these parameters were to investigate the numerical properties of the semi-Lagrangian approach and to have a quick benchmark versus PIC methods. Our results so far indicate that all features of the linear stage of the simulation are in very good agreement with PIC codes (growth rates and mode structures). The behaviour of the nonlinear stage is qualitatively similar to that given by PIC codes, but there remains a discrepancy to be resolved in the level of saturated mode amplitudes.

3. Effects of non-adiabatic electron dynamics and magnetic curvature

The non-uniformity of the magnetic field along the field line creates trapped particle populations and can affect microinstabilities in various ways. For example, trapped electrons tend to respond non-adiabatically, and their presence is overall destabilizing. In previous papers, it was shown that equilibrium radial electric fields and their associated $E \times B$

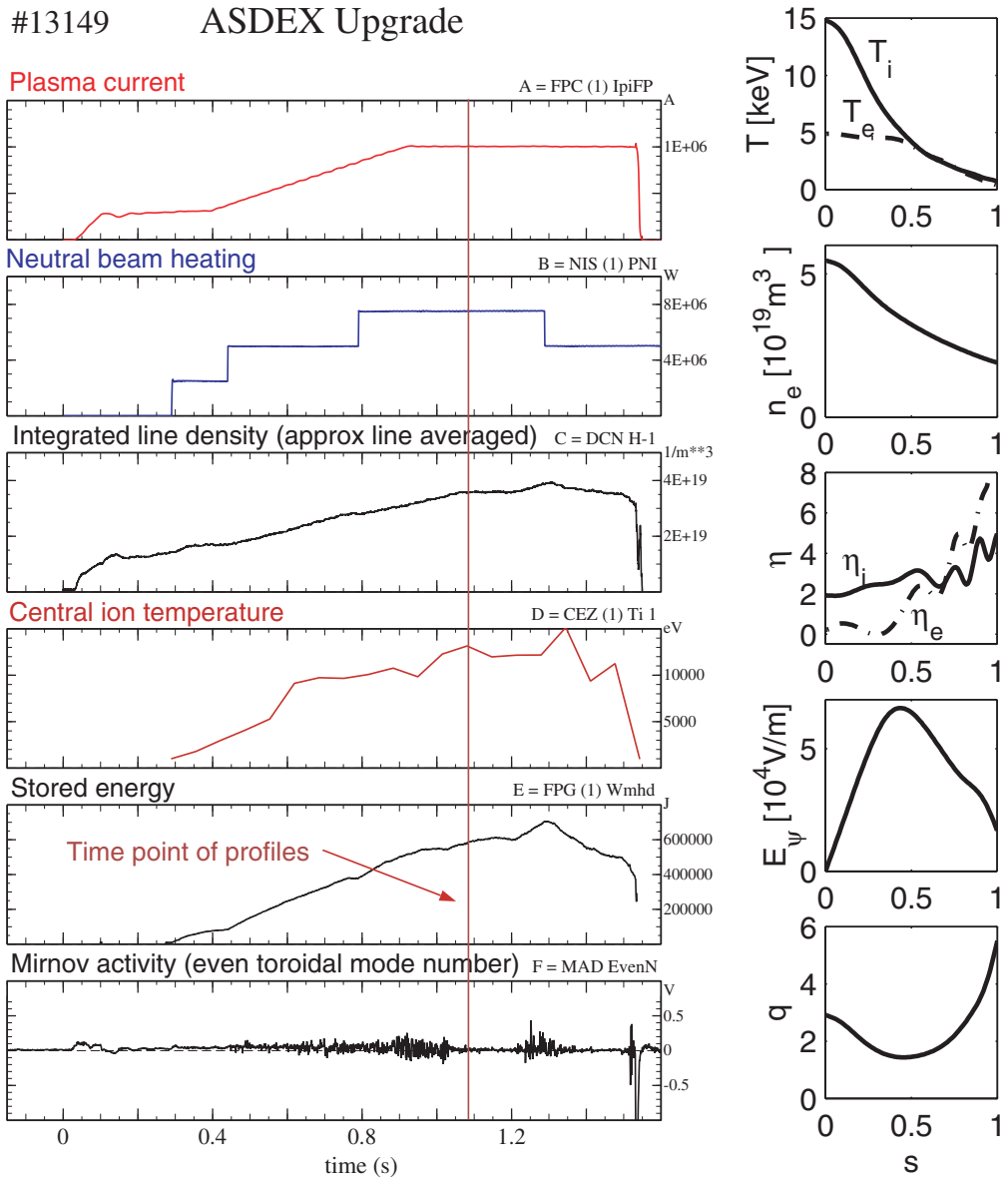

Figure 5. Time traces and equilibrium profiles of ASDEX-Upgrade shot no 13149.

flows in tokamak and heliac configurations stabilize toroidal, helical and slab ITG modes with a quadratic dependence on the shearing rate, whereas trapped particle modes can be destabilized by $E \times B$ flows [9, 19, 20]. We consider ASDEX-Upgrade shot no 13149, in which an ITB for ions was formed (figure 5). We study the global linear stability properties with a model that includes the non-adiabatic trapped electron response and the equilibrium radial electric fields [21]. Our full radius PIC δf code has been benchmarked with a global spectral gyrokinetic code [22]. Linear growth rates have been compared for the ASDEX-Upgrade case shown in this paper with those predicted by the transport model GLF23 [23]: there is agreement within a few per cent in the positive shear region of the plasma. The simulations were performed using 8 million ions, 8 million trapped electrons, $N_\psi = 128$, $N_\theta = 256$ and $\Delta t = 0.5\,\Omega_{\rm ci}^{-1}$. Considering the actual (reconstructed) ideal MHD equilibrium configuration and profiles of electron temperature and density but setting a uniform ion temperature and ignoring the radial electric field, E_ψ, the most unstable mode found is a trapped electron mode (figure 6, left). Considering also the actual $T_{\rm i}$ profile but still ignoring the radial electric field, we show in figure 6 (right) the most unstable mode found: it is a toroidal-ITG mode further destabilized by trapped electrons that is localized near the foot of the ion ITB. We then consider the equilibrium radial electric field and study the linear growth rate as a function of the Mach number of the $E \times B$ velocity by scaling the experimental profile by a series of constant factors. Figure 6 (right) shows that for the value inferred from experimental measurements (dashed line) the modes are completely stabilized. We have performed the computations using the assumption of a fully adiabatic electron response and repeated the calculations with adiabatic passing electrons but non-adiabatic (drift-kinetic) trapped electrons. In both cases full stabilization is reached when the equilibrium electric field is taken into account. The results of figure 6 are for a toroidal mode number $n = 30$,

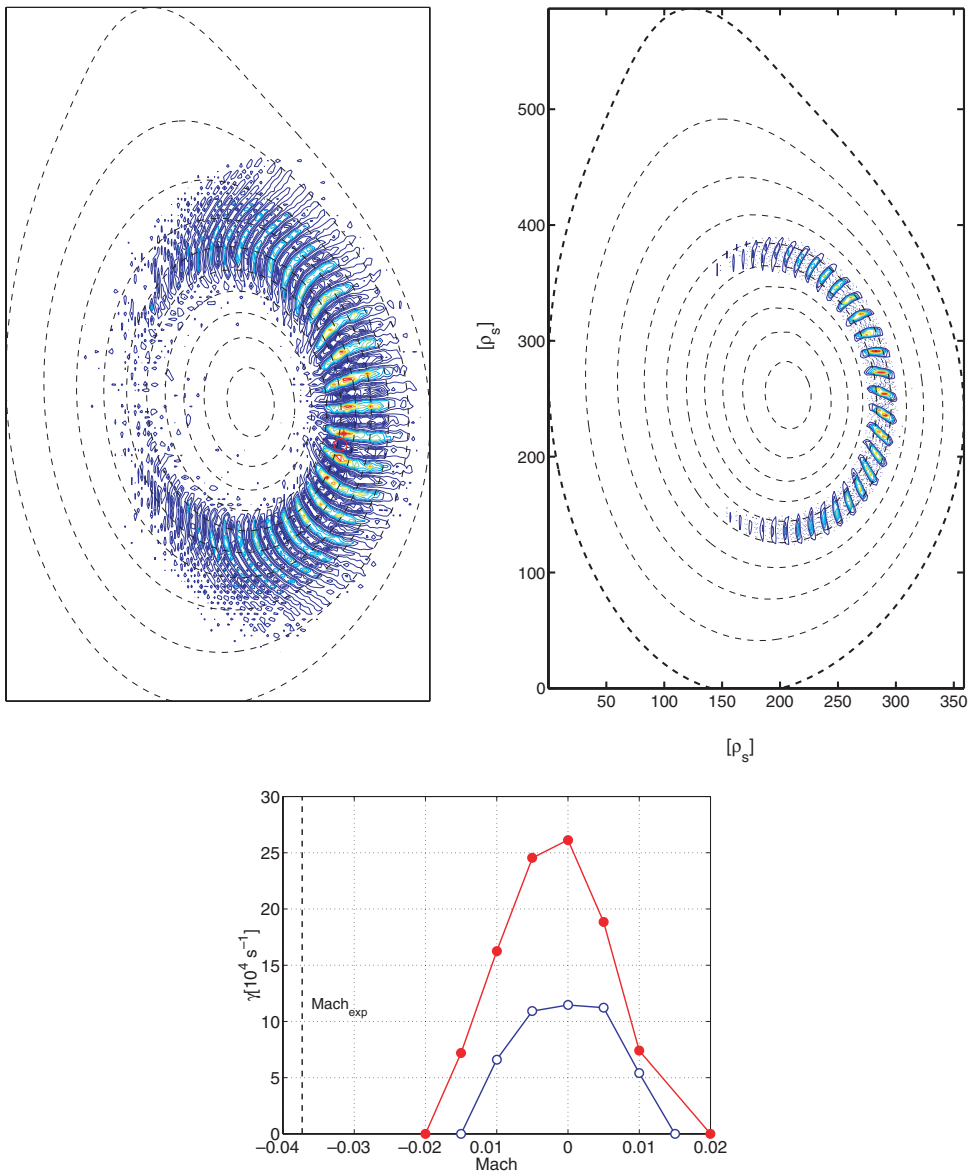

Figure 6. Top left: trapped electron mode calculated for ASDEX-Upgrade shot no 13149 assuming experimental equilibrium profiles except a flat T_i and no radial electric field. Top right: ITG mode calculated for ASDEX-Upgrade shot no 13149 assuming experimental profiles (including T_i) but no radial electric field. Left: growth rates of the most unstable mode versus equilibrium $E \times B$ velocity assuming adiabatic electrons (○) or drift-kinetic trapped electrons (●). - - - -: experimental Mach value.

which was chosen so that it corresponds to the highest growth rate without $E \times B$ flow. We have verified that for $n = 10$ and $n = 20$ the modes are also completely stabilized for the experimental values of radial electric fields.

In that experiment, the inferred ion heat diffusivity was improved not only at the ITB location but in the whole volume interior to it, a region of negative shear. In order to understand this, we have performed numerical simulations with all parameters as for the experiment, save for considering a temperature gradient localized around some region. Our results show that the ITG modes (including trapped electrons) are stable throughout the reversed shear region but unstable outside. The presence of the ITB in this shot is therefore compatible with $E \times B$ stabilization of ITG modes, even when the destabilizing non-adiabatic trapped electron response is considered. We have started the analysis of another ASDEX-Upgrade shot in which no ITB was formed. First results indicate that even when taking into account the equilibrium electric field, an unstable trapped electron mode subsists.

We now consider an axisymmetric bumpy equilibrium configuration with periodic boundary conditions so that it forms a topological torus [24]. Here, the dominant non-uniformity of B is a mirror term.

$$\vec{B}(r,z) = B_0\left[\frac{\vec{e}_r N c_0}{(2R_0) r \sin(Nz/R_0)} + \vec{e}_z\left(1 + c_0 \cos\left(\frac{Nz}{R_0}\right)\right)\right], \tag{2}$$

where $N = 5$ is the number of field periods, $R_0 = 5.5\,\mathrm{m}$ is the major radius of the topological torus, $a = 0.55\,\mathrm{m}$ is the minor radius and $B_0 = 2.5\,\mathrm{T}$. For $c_0 = 0.1$, one gets 28% trapped particles. These are typical parameters for the

W7-X stellarator. Both ions and electrons are modelled as fully gyrokinetic. The kinetic treatment of electrons affects the numerical behaviour of the simulation. First, it is an additional source of numerical noise. However, this is not too critical because we only performed linear calculations here. Second, there is a significant constraint on the time step, leading to a larger effort in computation time. In order to resolve the fast electron motion across the field bumpiness, the time step has to be decreased by a factor of about $\sqrt{m_e/m_i}$ as compared with simulations assuming adiabatic electrons. For the chosen parameters, this constraint is found to be strong enough to automatically satisfy another limit due to the electrostatic shear Alfvén wave [25], which is a high frequency mode with angular frequency, ω_H, given by the dispersion relation $\omega_H^2 = (m_i/m_e)(k_\parallel/k_\perp)^2\Omega_i^2$. The high computational cost in terms of number of time steps is compensated by using the optimized loading scheme described in section 2: numerical convergence with number of tracers is reached for $N = 64\,000$ with the same accuracy as for several million tracers with the unoptimized loading. The influence of the trapped particles and electron inertia is shown in figure 7. Considering an artificial $m_i/m_e = 100$ mass ratio, we observe that including the magnetic field bumpiness is overall destabilizing (diamonds in figure 7). However, as the mass ratio is increased, this destabilizing effect decreases and for the physical mass ratio becomes practically negligible (open triangles in figure 7). We note also that electron inertia is destabilizing even in the straight cylinder configuration. Finally, with a field bumpiness comparable with that of W7-X and for a real electron mass, we note that the ITG growth rates are very close to the adiabatic electron model prediction (circles in figure 7).

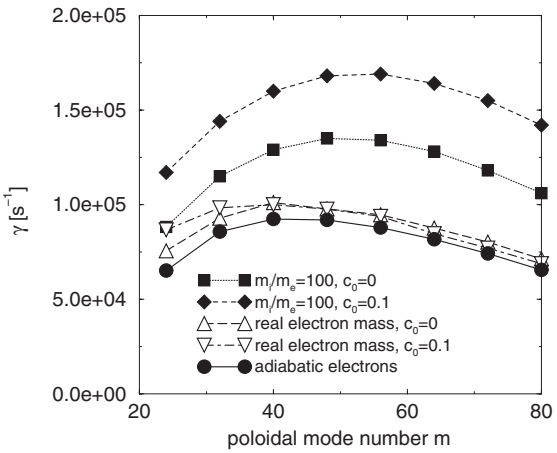

Figure 7. Growth rates of $n = 2$ modes versus m calculated for different bumpiness parameters, c_0 and ion to electron mass ratios, in a global simulation with both gyrokinetic ions and electrons, for W7-X-like parameters.

We have extended the global spectral approach of [22] to electromagnetic perturbations with a two-potential formulation $(\phi, A_\parallel)$ (thus neglecting the perturbed parallel magnetic field). All orders in ion Larmor radius are retained and non-adiabatic drift-kinetic electrons are included in the model. The formulation is applied to a large aspect ratio toroidal configuration [26] with the following parameters: $B_0 = 1\,\mathrm{T}$, $R_0 = 2\,\mathrm{m}$, $a = 0.5\,\mathrm{m}$, $q_0 = 1.25$, $q_a = 4.24$, equal T_i and T_e profiles with gradients peaking at $\rho/a = 0.6$ with $R/L_T = 10$ and $T(\rho/a = 0.6) = 7.5\,\mathrm{keV}$. Our results for a toroidal mode number $n = 7$ (figure 8, left) show that as β is increased, the toroidal-ITG growth rate decreases. At a β value about half the critical β limit for ideal MHD ballooning modes, another mode, called the toroidal AITG, is destabilized, qualitatively confirming earlier results [12, 13, 27]. The remarkable feature obtained with our global approach is the eigenmode structure. Figure 8 (right) shows the radial structure of the modulus of poloidal Fourier components of $A_\parallel$ for a toroidal AITG mode, $n = 7$ at $\beta = 6\%$. Noticeable are the sharp localized radial gradients in the vicinity of rational q surfaces (circles on top axis) for the corresponding poloidal component, $m = nq$. This means that the perturbed poloidal magnetic field has essentially a single poloidal mode number there and $k_\parallel \approx 0$. In between rational surfaces, the mode has a more ballooning-like structure with $k_\parallel \approx 1/qR$. This behaviour can be understood in the frame

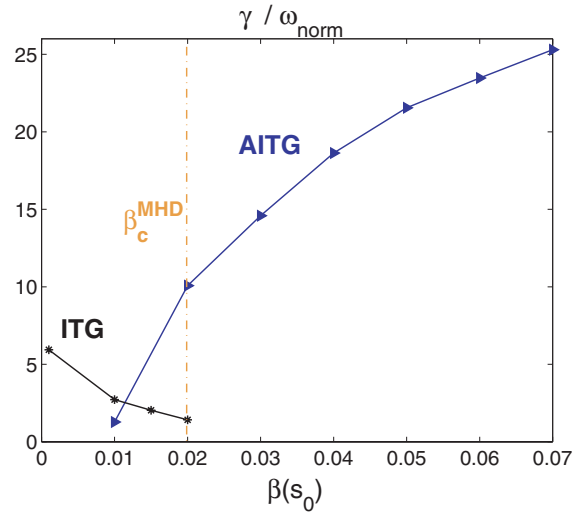

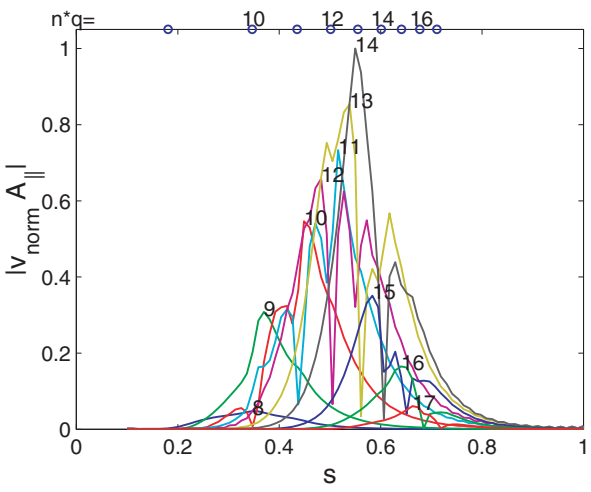

Figure 8. Left: growth rate of $n = 7$ toroidal ITG and AITG modes versus β, normalized to $\omega_{norm} = 3 \times 10^4\,\mathrm{s}^{-1}$. The critical β for ideal MHD ballooning is shown by the vertical line. Right: poloidal Fourier components of a $n = 7$ toroidal AITG eigenmode at $\beta = 6\%$ versus normalized minor radius, $s = \rho/a$, showing the resonant behaviour at rational q values, indicated by the circles on the top axis.

of our gyrokinetic theory as follows: electron contributions to the perturbed distribution function can be obtained in terms of plasma dispersion functions, the argument of which, $\omega/k_\parallel v_{\rm the}$, varies strongly radially in the vicinity of rational magnetic surfaces. The radial width, $\Delta\rho$, of the region where the argument is larger than unity can be estimated as $\Delta\rho/\rho \approx R(q/\hat{s})(|\omega|/v_{\rm the}|m|)$, where $\hat{s}$ is the magnetic shear. It is of course necessary to have a finer radial mesh size than $\Delta\rho$ in order to resolve this sharp behaviour. We have checked that increasing the number of radial mesh intervals from 128 as used for figure 8 up to 512, the sharp radial structure is numerically converged. We note that such a radial structure for the toroidal AITG modes shown in this paper cannot be found with electron fluid models. It is of course inaccessible to local models that assume, e.g. $k_\parallel \approx 1/qR$ or to models based on first order ballooning approximation. The sharp radial structure implies that $k_\perp \rho_{\rm Li} \sim 1$, and thus models that use low order expansions in $k_\perp \rho_{\rm Li}$ may be inaccurate. Our approach overcomes all these difficulties.

4. Discussion and future directions of work

We have demonstrated the pertinence of using the energy conservation principle as an indicator of the quality of nonlinear global gyrokinetic simulations. The optimized loading technique is very effective in improving this quality. For PIC simulations, the main problem is numerical noise resulting from phase space sampling, which is at the heart of the method. As shown in [15], the statistical error is $\sigma/\sqrt{N}$, where σ is the variance of the estimator. The optimized loading scheme seeks to minimize the error by reducing σ, thus providing an invaluable tool in circumstances where computer memory limitations prohibit increasing N. We have observed a clear correlation between the achieved accuracy of the energy conservation and that of other important physical quantities such as the heat flux or the zonal component of the perturbation.

The importance of retaining the $v_\parallel$ nonlinearity has also been evidenced. As rigorously established in [28], this is necessary in order to ensure that conservation properties are satisfied, whatever the geometry or size of the system. We have shown an example in cylindrical geometry of how neglecting it leads to an incorrect zonal $E \times B$ flow structure because of the loss of the charge conservation property. Consequently, the calculated heat flux is also incorrect. Moreover, the system loses its energy conservation property, and a very useful indicator of the quality of simulations is lost. It may be possible, however, that in toroidal geometry or larger systems the quantitative effect of neglecting the parallel nonlinearity is reduced. A definitive answer to this issue will only be made once nonlinear, noise-free simulations in toroidal geometry that retain this nonlinearity are performed and compared with similar simulations that neglect it.

The pivotal role of the zonal component of the perturbation has been confirmed. We have shown how the system establishes a particular radial structure with regions of reduced heat flux alternating with regions of higher heat flux. The zonal component of the electric field, once this structure is established, stays quasi-steady on much longer timescales as compared with the inverse linear growth rates of ITG modes. The question arises as to how to use the global gyrokinetic results for transport modelling. A local diffusion coefficient can obviously not reproduce the observed nonlocal, structured features of heat flux. The optimized loading scheme has very recently been implemented in the toroidal version of the code, and first results indicate that it does also improve the quality of the simulations [29].

We have shown the consistency of the presence of an ITB in an ASDEX-Upgrade experiment with the $E \times B$ stabilization, even when the usually destabilizing non-adiabatic trapped electron response was taken into account. First results on another ASDEX-Upgrade discharge in which no ITB was formed indicate that a trapped electron mode is still unstable even when the experimental profile of equilibrium radial electric field is considered. A more detailed analysis will be performed in the future.

We have shown that trapped electron dynamics is only weakly destabilizing ITG modes in a bumpy configuration modelling W7-X. Global gyrokinetic computations using the full three-dimensional geometry of the equilibrium magnetic field [30] show that ITG modes are rather weakly coupled by three-dimensional geometrical effects in W7-X [31] and growth rates are close to those obtained in a straight cylinder. This gives some justification for the relevance of the simplest geometry (cylinder) and the simplest electron model (adiabatic) used in our nonlinear simulations. Of course, more work is needed to ascertain this hypothesis.

We have shown that the inclusion of electron dynamics and electromagnetic effects creates a resonant radial structure of the unstable modes at rational q values. Further work, in particular nonlinear global electromagnetic gyrokinetic simulations, may well be needed before concluding that this could be related to the resonant behaviour of electron transport observed in some tokamaks. Even though it should be recalled that all the results presented in this paper were calculated without collisional effects, it is interesting to note that the resonant behaviour at rational q surfaces of the electromagnetic modes we found resembles that of tearing modes.

Acknowledgments

Fruitful discussions with Drs T.S. Hahm and Y. Idomura are gratefully acknowledged. This work was partly supported by the Swiss National Science Foundation.

References

[1] Dimits A.M. *et al* 2000 *Phys. Plasmas* **7** 969
[2] Hammett G.W., Beer M.A., Dorland W., Cowley S.C. and Smith S.A. 1993 *Plasma Phys. Control. Fusion* **35** 973
[3] Sydora R.D., Decyck V.K. and Dawson J.M. 1996 *Plasma Phys. Control. Fusion* **38** A281
[4] Lin Z., Hahm T.S., Lee W.W., Tang W.M. and White R.B. 1998 *Science* **281** 1835
[5] Rosenbluth M.N. and Hinton F.L. 1998 *Phys. Rev. Lett.* **80** 724
[6] Hahm T.S. 1996 *Phys. Plasmas* **3** 4658
[7] Dimits A.M. and Lee W.W. 1993 *J. Comput. Phys.* **107** 309
[8] Hatzky R., Tran T.M., Könies A., Kleiber R. and Allfrey S.J. 2002 *Phys. Plasmas* **9** 898
[9] Allfrey S.J., Bottino A., Sauter O. and Villard L. 2002 *New J. Phys.* **4** paper no.29, http://www.njp.org
[10] Allfrey S.J. *et al* 2002 *Proc. 29th EPS Conf. on Plasma Physics and Controlled Fusion (Montreux, Switzerland, June 2002)* vol 26A, ed R. Behn and C. Varandas

(*Europhysics Conference Abstracts*) (Geneva: European Physical Society) p P4.059, http://epsppd.epfl.ch
[11] Allfrey S.J. *et al* 2002 *Proc. Joint Varenna-Lausanne International Workshop on Theory of Fusion Plasmas (Varenna, August 2002)* ed J.W. Connor *et al* ISPP-20 (Bologna: Editrice Compositori) p 171
[12] Kim J.Y., Horton W. and Dong J.Q. 1993 *Phys. Fluids* B **5** 4030
[13] Zonca F., Chen L., Dong J.Q. and Santoro R.A. 1999 *Phys. Plasmas* **6** 1917
[14] Fivaz M. *et al* 1998 *Comput. Phys. Commun.* **111** 27
[15] Allfrey S.J. and Hatzky R. 2003 *Comput. Phys. Commun.* **154** 98
[16] Jenko F. and Scott B.D. 1998 *Phys. Rev. Lett.* **80** 4883
[17] Brunetti M. *et al* 2002 *Proc. 29th EPS Conf. on Plasma Physics and Controlled Fusion (Montreux, Switzerland, June 2002)* vol 26A, ed R. Behn and C. Varandas (*Europhysics Conference Abstracts*) (Geneva: European Physical Society) p P4.102, http://epsppd.epfl.ch
[18] Grandgirard V. *et al* 2002 *Proc. 29th EPS Conf. on Plasma Physics and Controlled Fusion (Montreux, Switzerland, June 2002)* vol 26A, ed R. Behn and C. Varandas (*Europhysics Conference Abstracts*) (Geneva: European Physical Society) p P4.095, http://epsppd.epfl.ch
[19] Villard L., Bottino A., Sauter O. and Vaclavik J. 2002 *Phys. Plasmas* **9** 2684
[20] Villard L. *et al* 2002 *Proc. 29th EPS Conf. on Plasma Physics and Controlled Fusion (Montreux, Switzerland, June 2002)* vol 26A, ed R. Behn and C. Varandas (*Europhysics Conference Abstracts*) (Geneva: European Physical Society) p P4.069, http://epsppd.epfl.ch
[21] Bottino A. *et al* 2002 *Proc. 29th EPS Conf. on Plasma Physics and Controlled Fusion (Montreux, Switzerland, June 2002)* vol 26A, ed R. Behn and C. Varandas (*Europhysics Conference Abstracts*) (Geneva: European Physical Society) p P1.040, http://epsppd.epfl.ch
[22] Brunner S., Fivaz M., Tran T.M. and Vaclavik J. 1998 *Phys. Plasmas* **5** 3929
[23] Waltz R.E. *et al* 1997 *Phys. Plasmas* **4** 2482
[24] Sorge S. and Hatzky R. 2002 *Plasma Phys. Control. Fusion* **44** 2471
[25] Lee W.W. 1987 *J. Comput. Phys.* **72** 243
[26] Falchetto G.L., Vaclavik J. and Villard L. 2003 *Phys. Plasmas* **10** 1424
[27] Dong J.Q., Chen L. and Zonca F. 1999 *Nucl. Fusion* **39** 1041
[28] Hahm T.S. 1988 *Phys. Fluids* **31** 2670
[29] Bottino A. *et al* 2002 *Theory of Fusion Plasmas: Proc. Joint Varenna-Lausanne International Workshop (Varenna, August 2002)* ed J.W. Connor *et al* ISPP-20 (Bologna: Editrice Compositori) p 351
[30] Jost G., Tran T.M., Cooper W.A., Villard L. and Appert K. 2001 *Phys. Plasmas* **8** 3321
[31] Allfrey S.J., Bottino A., Hatzky R., Jost G. and Villard L. 2001 *Proc. 28th EPS Conf. on Controlled Fusion and Plasma Physics (Funchal, Madeira, Portugal, June 2001)* vol 25A, ed C. Silva *et al* (*Europhysics Conference Abstracts*) (Geneva: European Physical Society) p P5.042, http://epsppd.epfl.ch